Traffic 2009; **10:** 637–647
Blackwell Munksgaard

doi: 10.1111/j.1600-0854.2009.00897.x

14-3-3 Ligand Prevents Nuclear Import of c-ABL Protein in Chronic Myeloid Leukemia

Manuela Mancini[1]*, Nevena Veljkovic[2], Valentina Corradi[3], Elisa Zuffa[1], Patrizia Corrado[1], Eleonora Pagnotta[4], Giovanni Martinelli[1], Enza Barbieri[5] and Maria Alessandra Santucci[1]

[1] *Istituto di Ematologia e Oncologia Medica 'Lorenzo e Ariosto Serágnoli', University of Bologna-Medical School, Bologna, Italy*
[2] *Center for Multidisciplinary Research, Institute of Nuclear Sciences Vinca, Belgrade, Serbia*
[3] *Dipartimento Farmaco Chimico Tecnologico, University of Siena, Siena, Italy*
[4] *Research Center for Industrial Crops, Bologna, Italy*
[5] *Istituto di Radioterapia 'Luigi Galvani', University of Bologna-Medical School, Bologna, Italy*
**Corresponding author: Manuela Mancini, mancini_manu@yahoo.com*

Here we demonstrated that the 'loss of function' of not-rearranged c-ABL in chronic myeloid leukemia (CML) is promoted by its cytoplasmic compartmentalization bound to 14-3-3 sigma scaffolding protein. In particular, constitutive tyrosine kinase (TK) activity of p210 BCR-ABL blocks c-Jun N-terminal kinase (JNK) phosphorylation leading to 14-3-3 sigma phosphorylation at a critical residue (Ser^{186}) for c-ABL binding in response to DNA damage. Moreover, it is associated with 14-3-3 sigma over-expression arising from epigenetic mechanisms (promoter hyper-acetylation). Accordingly, p210 BCR-ABL TK inhibition by the TK inhibitor Imatinib mesylate (IM) evokes multiple events, including JNK phosphorylation at Thr^{183}, p38 mitogen-activated protein kinase (MAPK) phosphorylation at Thr^{180}, c-ABL de-phosphorylation at Ser residues involved in 14-3-3 binding and reduction of 14-3-3 sigma expression, that let c-ABL release from 14-3-3 sigma and nuclear import, and address BCR-ABL-expressing cells towards apoptotic death. Informational spectrum method (ISM), a virtual spectroscopy method for analysis of protein interactions based on their structure, and mathematical filtering in cross spectrum (CS) analysis identified 14-3-3 sigma/c-ABL binding sites. Further investigation on CS profiles of c-ABL- and p210 BCR-ABL-containing complexes revealed the mechanism likely involved 14-3-3 precluded phosphorylation in CML cells.

Key words: Chronic Myeloid Leukemia (CML), BCR-ABL, Imatinib mesylate (IM), c-ABL,14-3-3 sigma, JNK, p38 MAPK

Received 4 April 2008, revised and accepted for publication 5 February 2009, uncorrected manuscript published online 11 February 2009, published online 19 March 2009

The BCR-ABL gene, originated from the rearrangement of c-ABL gene on chromosome 9 with BCR sequences on chromosome 22, is the molecular hallmark and the causative event of chronic myeloid leukemia (CML). It encodes a p210 kDa protein where ABL tyrosine kinase (TK) is constitutively activated by the BCR coiled-coil oligomerization domain (1). In consequence of its cytoplasmic location p210 BCR-ABL, TK promotes proliferation and survival of CML progenitors. Moreover, it usurps c-ABL physiological functions in response to stress, which are conditional upon nuclear translocation and interactions with nuclear effectors of growth arrest and apoptosis (2). Accordingly, p210 BCR-ABL nuclear entrapment by nuclear export inhibitor leptomycin B restores the pro-apoptotic function of rearranged c-ABL (3). However, the 'loss of function' of residual, not-rearranged c-ABL protein in CML cells is still elusive. It might result from transcriptional or post-transcriptional events that lower c-ABL levels, including DNA hyper-methylation at c-ABL promoter or downregulation of ABL-interacting proteins through the ubiquitin-dependent proteasome machinery, but neither mechanism has been definitively ascertained (4,5).

The c-ABL protein is a non-receptor TK implicated in many cell processes, including cell cycle progression, survival, adhesion and motility. In response to DNA damage it is activated by the ataxia teleangectasia mutated (ATM) gene product through phosphorylation at a serine residue (Ser^{465}) located within the kinase domain and intramolecular events, and targeted to the nuclear compartment where it interacts with many components of response to stress (6,7). C-ABL nuclear relocation is preceded by its release from 14-3-3 scaffolding proteins promoted by c-Jun N-terminal kinase (JNK) phosphorylation at Ser^{184} near the ligand-binding groove RSXpS/TXP that regulates 14-3-3 binding to client proteins (8).

Here we demonstrated that p210 BCR-ABL TK precludes JNK and 14-3-3 sigma phosphorylation in response to ionizing radiation (IR), the prerequisite for c-ABL nuclear relocation. Inhibition of the fusion protein enzymatic activity by the TK inhibitor IM (also referred to as STI571 or Glevec) is followed by JNK and 14-3-3 sigma phosphorylation, c-ABL release and nuclear import. Informational spectrum method (ISM) is a virtual spectroscopy method for functional analysis of protein interactions, based on their structure and mathematical filtering in cross spectrum (CS) analysis. ISM identified 14-3-3 sigma/c-ABL binding sites at a 14-3-3 sigma domain (spanning residues 111–155) and three c-ABL domains (spanning residues 185–209, 548–572 and 729–753) (9,10). Moreover, CS profiles suggested that stronger JNK

binding to p210 BCR-ABL/histone deacetylase 1 (HDAC1) complex described in our previous study (11) might hinder JNK targeting to c-ABL/14-3-3 sigma complex.

Results

P210 BCR-ABL TK prevents the nuclear import of not-rearranged c-ABL protein in response to IR through mechanisms encompassing JNK and 14-3-3 sigma phosphorylation

The nuclear import of c-ABL protein and its activation by nuclear ATM are early responses to radio-induced DNA damage (12). We investigated the impact of p210 BCR-ABL TK on sub-cellular redistribution of the product of c-ABL allele not involved in the rearrangement with BCR. C-ABL location was investigated at 3 h from exposure to low dose (4 Gy), low dose rate (0.05 Gy/min) gamma irradiation in a 32D cell clone (3B) transducing a temperature-sensitive (ts) BCR-ABL construct (constitutive TK activity only at the permissive temperature of 33°C) and K562 cell line. The absence of p210 BCR-ABL phosphorylation at Tyr^{245} (in the SH2-linker domain, proceeding fromTyr^{412} phosphorylation in the activation loop) in clone 3B kept at 39°C confirmed that p210 BCR-ABL TK is not active under non-permissive temperature conditions (Figure 1) (11). The nuclear import of p145 c-ABL protein in response to IR was seen in parental 32D cell line and clone 3B kept at 39°C, but not in clone 3B kept at 33°C and K562 cell line (Figure 1). In all instances IR did not influence the expression of p145 c-ABL protein in the cytoplasm (Figure 1). P210 BCR-ABL protein was stably confined to the cytoplasm since the 1-24 h from exposure to IR in clone 3B kept at either temperature and K562 cell line, and both its levels and phosphorylation did not undergo any significant change (Figure 1 and data not shown).

C-ABL protein is retained in the cytoplasm by the ligand to a conserved RSXpS/TXP motif of 14-3-3 scaffolding proteins, mediated by Thr^{735} phosphorylation that interferes with its nuclear import by blocking nuclear localization signals (NLS) (13,14). Its nuclear targeting in response to DNA damage is promoted by 14-3-3 sigma phosphorylation at Ser^{186} (corresponding to Ser^{184} in 14-3-3 zeta) by JNK (8). In the absence of p210 BCR-ABL expression (32D parental cell line) or TK activity (clone 3B kept at 39°C), c-ABL nuclear import in response to IR was associated with enhanced phosphorylation of 14-3-3 sigma at Ser^{186} and JNK at a threonine residue (Thr^{183} adjacent to Ser^{184}) (Figure 1). JNK-increased expression following IR exposure likely arises from its enhanced stability associated with phosphorylation (15). Moreover, a significant reduction of c-ABL phosphorylation at two different Ser-containing motifs involved in 14-3-3 binding and of c-ABL/14-3-3 sigma co-immunoprecipitation signals was apparent in irradiated 32D cell line and clone 3B kept at 39°C (Figure 1) (16). In clone 3B kept at 33°C and K562 cell line, none of above-mentioned signals was affected by IR exposure, supporting that p210 BCR-ABL TK precludes c-ABL nuclear import in response to DNA damage by blocking the sequence of events that allowed c-ABL dissociation from cytoplasmic 14-3-3 (Figure 1).

Notably, in clone 3B kept at 33°C 14-3-3 sigma expression was higher compared with 32D parental cell line and clone 3B at 39°C supporting a fusion protein impact on scaffolding protein expression. The matter is addressed in the following paragraph.

Nuclear import and pro-apoptotic activity of c-ABL protein are promoted by p210 BCR-ABL TK inhibition by IM and further enhanced by 14-3-3 ligand inhibition

The impact of p210 BCR-ABL TK on c-ABL partitioning between sub-cellular compartments was investigated at various intervals of exposure to 1 μM IM. In clone 3B at 33°C, IM abrogated p210 BCR-ABL phosphorylation at Tyr^{245} from 2-24 h, but neither influenced fusion protein expression nor allowed its nuclear import (Figure 2A). A significant increment of p145 c-ABL protein in the nuclear compartment was apparent at 24 h of IM exposure (Figure 2A). It was associated with the progressive reduction of c-ABL in the cytoplasm and phosphorylation at Ser residues involved in 14-3-3 binding, as well as of c-ABL/14-3-3 co-immunoprecipitation signals (17). P145 c-ABL nuclear relocation in response to IM followed persistent phosphorylation of 14-3-3 sigma at Ser^{186}, the critical residue for c-ABL cytoplasmic ligand, and the activating phosphorylation of JNK at Thr^{183} and p38 mitogen-activated protein kinase (MAPK) at Thr^{180} (Figure 2A). The significant reduction of 14-3-3 sigma in the cytoplasm at 24 h of IM exposure further supports p210 BCR-ABL TK impact on scaffolding protein expression (Figure 2A).

To address the role of 14-3-3 ligand in c-ABL release and nuclear targeting we used R18, a 20-mer peptide extensively contacting the hydrophobic side of conserved 14-3-3 amphipatic groove in a phosphorylation-independent way (18). In clone 3B at 33°C nuclear c-ABL levels were raised by 24-h exposure to R18 (25 μM) alone, although to a lesser extent compared with IM, and further increased by IM combination (Figure 2B). Conversely, R18 either alone or in combination with IM left p210 BCR-ABL confined to the cytoplasm (Figure 2B). The induction of all the above-mentioned signals and c-ABL nuclear import in response to IM and R18 was confirmed in K562 cell line by means of protein resolution in SDS-PAGE and confocal microscopic analysis (data not shown and Figure 2C).

Apoptotic death, proceeding from the activation of nuclear proteins p53, p73 and Rad9, is a major consequence of c-ABL targeting the nuclear compartment (19). Accordingly, in clone 3B at 33°C and K562 cell line the apoptotic cell fraction was significantly increased by R18 and IM alone, and further augmented by the two drug combination (Figure 2D).

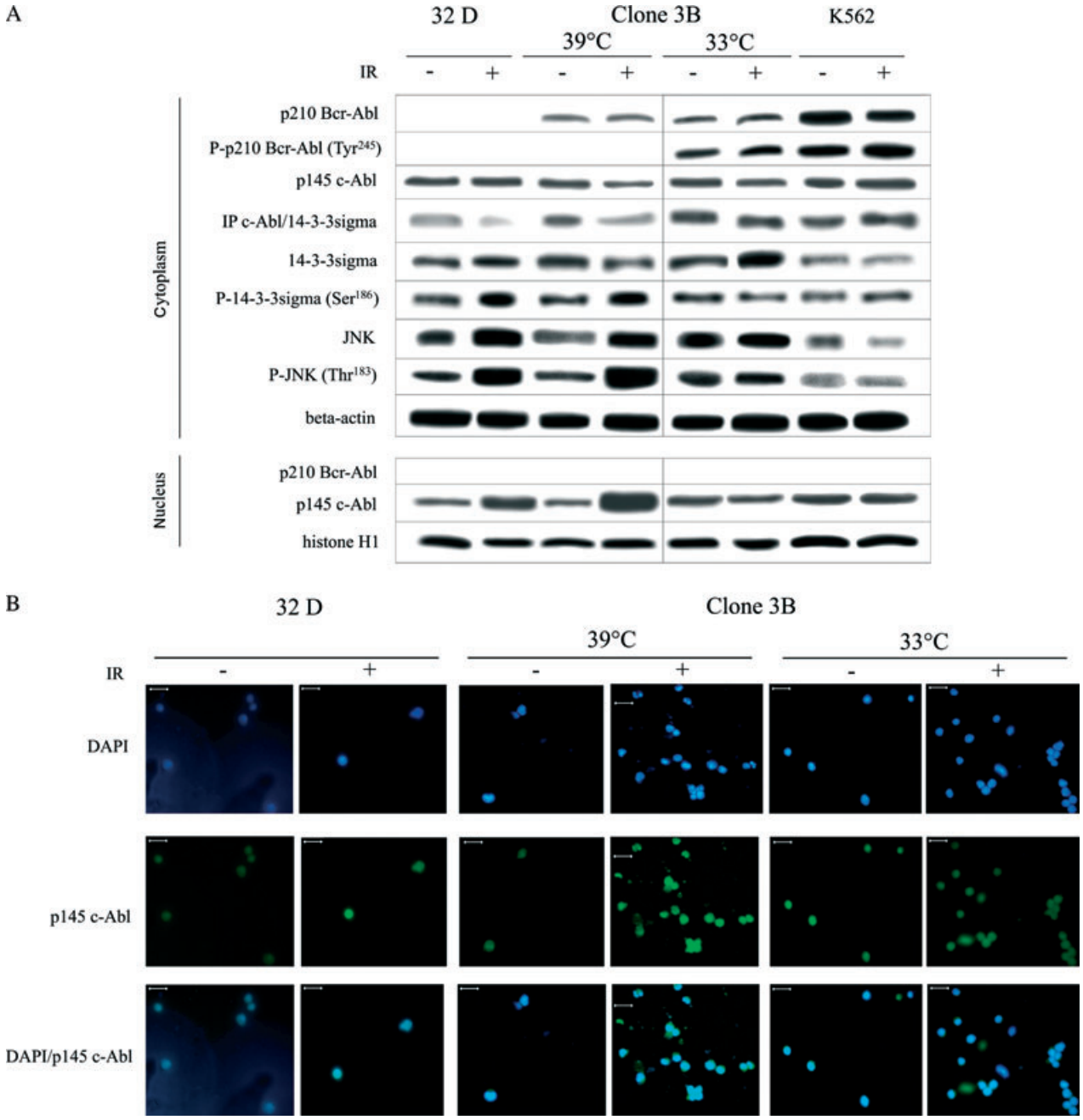

Figure 1: P210 BCR-ABL TK prevents the nuclear import of not-rearranged p145 c-ABL through mechanisms precluding the release from 14-3-3 sigma. Protein expression in cytoplasmic and nuclear compartments of parental murine myeloid progenitor cell line 32D, ts p210 BCR-ABL-transduced clone 3B kept at permissive (33°C) and non-permissive (39°C) temperature for p210 BCR-ABL TK activity and K562 cell line was investigated at 3rd h from exposure to low dose (4 Gy)/low dose rate (0.05 Gy/min) gamma irradiation by means of western blot and IP/immunoblotting. Beta-actin and histone H1 served as controls for protein loading. Signal intensities in single blots were measured by a GS-700 imaging densitometer. Results presented here have been confirmed in two additional experiments. C-ABL nuclear import in response to IR was confirmed in 32D, in clone 3B kept at 39°C and at 33°C by means of confocal microscopic analysis. Green colour indicates c-ABL protein, while blue colour represents nuclear compartment, labelled with DAPI.

14-3-3 sigma phosphorylation in response to IM is concurrently promoted by JNK and p38 MAPK

JNK and p38 MAPK have major roles in phosphorylation of 14-3-3 proteins. In particular, JNK-activating phosphorylation at Ser^{184} induces 14-3-3 phosphorylation at critical residue for c-ABL ligand, while p38 MAPK is involved in 14-3-3 phosphorylation at inhibitory Ser residues of dimerization and stable binding to client

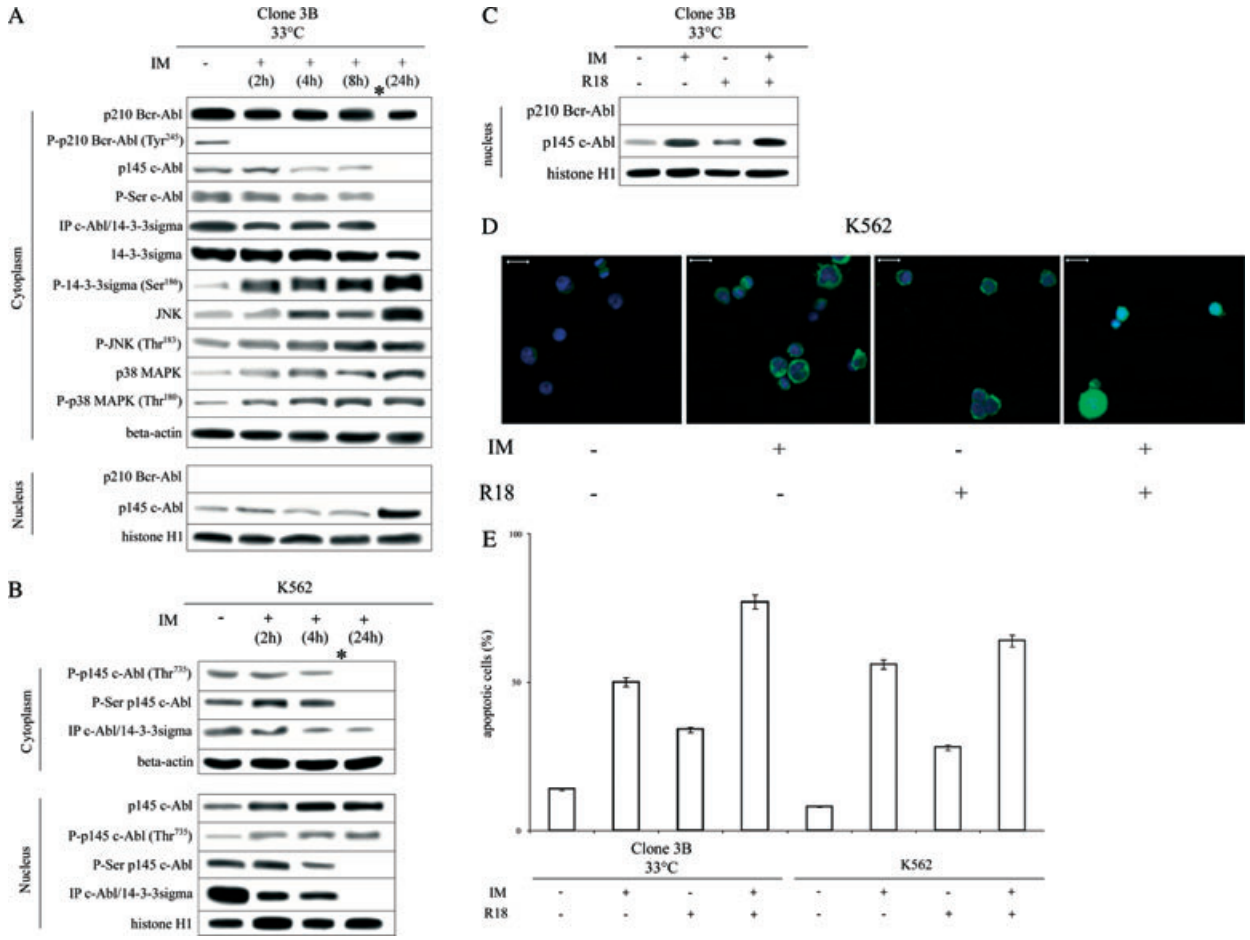

Figure 2: 14-3-3 sigma ligand is involved in c-ABL cytoplasmic compartmentalization and loss of pro-apoptotic function associated with p210 BCR-ABL TK. A) Protein expression in cytoplasmic and nuclear compartments of clone 3B kept at the permissive temperature (33°C) for p210 BCR-ABL TK activity was investigated at the 2, 4, 8 and 24 h of exposure to 1 μM IM. See legend to Figure 1 for details. The asterisk marks the different points of the blot where a signal (corresponding to 12 h of treatment with IM), not considered in our discussion because irrelevant, was deleted.hb B) C-ABL nuclear translocation in clone 3B kept at 33°C was investigated at 24 h of exposure to 25 μM R18 and 1 μM IM. See legend to Figure 1 for details. C) C-ABL nuclear import in response to IM (1 μM) and R18 (25 μM), either alone or associated, was confirmed in K562 cell line by means of confocal microscopic analysis. Green colour indicates c-ABL protein, while blue colour represents nuclear compartment, labelled with DAPI. D) Apoptotic death induction following 24-h exposure to IM and R18 was assayed in clone 3B at 33°C and K562 cell line by means of cytofluorimetric analysis of Annexin V and PI uptake. Results presented here are the mean of three repeated experiments ± SD.

proteins (8,20). Specific inhibitors of JNK (JNK inhibitor IX) and p38 MAPK (SB202190) were used to investigate JNK and p38 MAPK individual contribution to 14-3-3 sigma phosphorylation in BCR-ABL-expressing cell response to IM. Significant reduction of JNK phosphorylation at Thr^{183} and p38 MAPK phosphorylation at Thr^{180} following a 24-h exposure to JNK and p38 MAPK inhibitors of clone 3B kept at 33°C proved the two compound efficacy on their targets (Figure 3A). Both inhibitors did not affect p210 BCR-ABL expression, phosphorylation and sub-cellular location, p145 c-ABL protein expression in the cytoplasm and 14-3-3 sigma levels (Figure 3A and data not shown). Conversely, they significantly reduced 14-3-3 sigma phosphorylation at Ser^{186} in response to IM and lessened, but did not abrogate, p145 c-ABL nuclear import (Figure 3A). Notably, JNK and p38 MAPK inhibitors prevented c-ABL complete de-phosphorylation at Ser residues critical for 14-3-3 binding in response to IM (Figure 3A). C-ABL persistent phosphorylation and 14-3-3 sigma steady levels might concur to retain c-ABL in the cytoplasm bound to 14-3-3 sigma following combined exposure to IM and JNK or p38 MAPK inhibitors (Figure 3A). Unexpectedly, JNK inhibitor significantly increased apoptotic death in response to IM, while p38 MAPK inhibitor had no effects on survival of IM-treated cells (Figure 3B).

14-3-3 sigma over-expression associated with p210 BCR-ABL TK activity arises from epigenetic mechanisms

Higher levels of 14-3-3 sigma in clone 3B at 33°C compared with 32D parental cell line and clone 3B at 39°C,

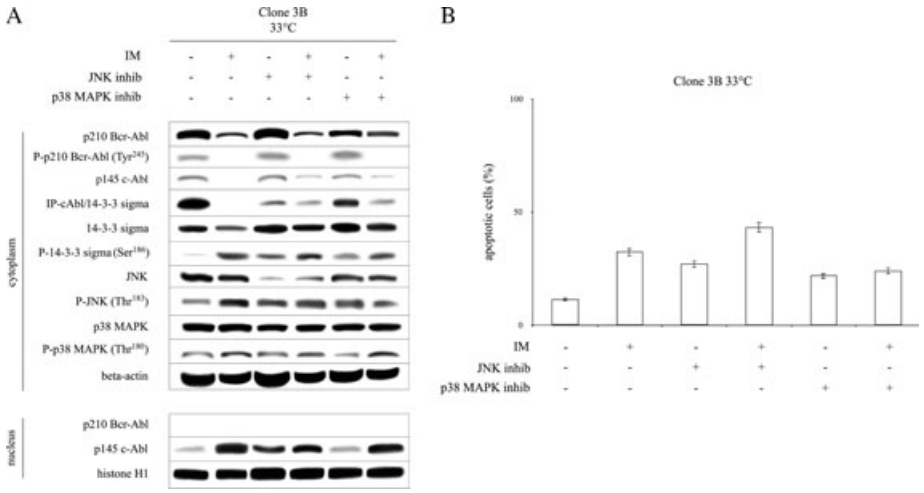

Figure 3: 14-3-3 sigma phosphorylation in response to IM is concurrently promoted by JNK and p38 MAPK. A) Protein expression in cytoplasmic and nuclear compartments of clone 3B kept at 33°C was investigated at 24 h of exposure to IM (1 μM) alone or associated with JNK inhibitor (20 μM) and p38 MAPK inhibitor (20 μM). See legend to Figure 1 for details. B) Apoptotic death induction in response to IM, JNK and p38 MAPK inhibitors. See legend to Figure 2D for details.

and its reduction in response to IM suggest that p210 BCR-ABL TK may influence the scaffolding protein expression (Figures 1 and 2A). To quantify 14-3-3 sigma expression we used a semi-quantitative polymerase chain reaction (PCR) strategy exploiting the ratio between 14-3-3 sigma and housekeeping G3PDH amplification signals. In clone 3B at 33°C and K562 cell line, 14-3-3 sigma expression relative to G3PDH was significantly reduced 2 and 8 h of exposure to IM, respectively, up to 24 h (Figure 4A). In both cell types 14-3-3 sigma transcript reduction preceded protein reduction, which became apparent at 24 h of IM exposure (Figure 4A). This discrepancy might be because of events affecting protein translation or stability.

To elucidate whether epigenetic mechanisms play a role in 14-3-3 sigma transcription, we investigated histone H4 acetylation status at a 14-3-3 sigma promoter region critical for gene transcription (21). PCR amplification on DNA purified from anti-acetylated histone H4 ChIP products allowed assessing of the levels of 14-3-3 sigma promoter acetylation relative to constitutively acetylated histone H4 as internal control (11). To avoid the risk of misleading

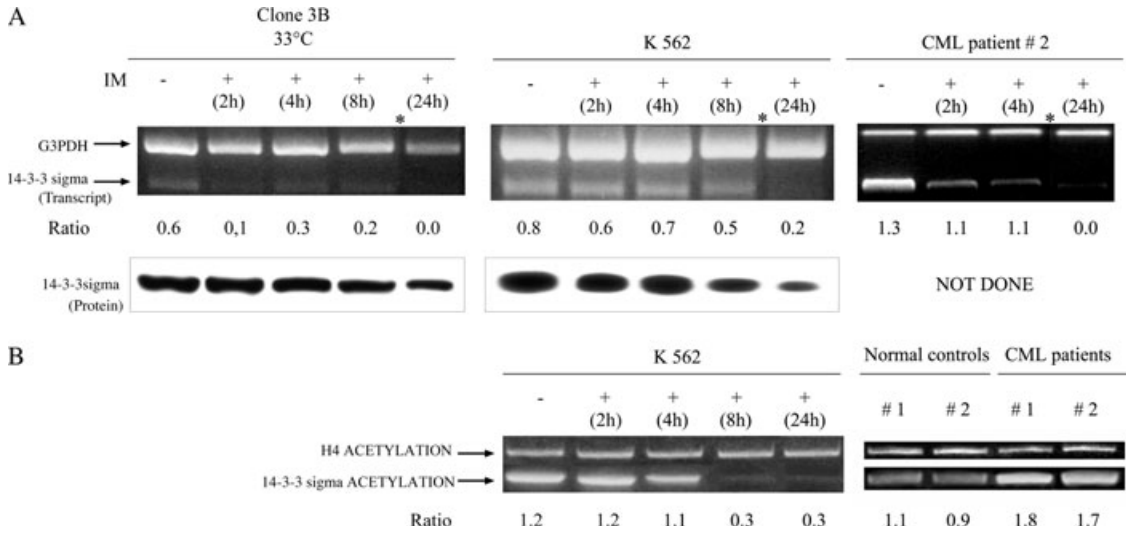

Figure 4: 14-3-3 sigma over-expression associated with p210 BCR-ABL TK is because of histone H4 hyper-acetylation at a 14-3-3 sigma promoter region critical for gene transcription. A) Expression of 14-3-3 sigma was investigated by means of a semi-quantitative PCR strategy exploiting the ratios between 14-3-3 sigma and housekeeping G3PDH amplification signals in clone 3B at 33°C (upper left panel), K562 cell line (middle upper panel) and CD34+ cells from a CML patient (# 2) at diagnosis (right upper panel) either untreated or at various intervals of exposure to IM. Lower left and middle panels indicate protein levels. As in figure 2, the asterisk marks the different points of the gel where a signal (corresponding to 12 h of treatment with IM), not-considered in our discussion because irrelevant, was deleted. B) Acetylation status of 14-3-3 sigma promoter relative to the constitutively acetylated histone H4 as internal control was investigated in K562 cells line (left panel) and CD34+ cells from two normal controls (peripheral blood apheresis intended for bone marrow transplantation) and two CML patients at diagnosis (right panel) by means of PCR amplification of DNA purified from anti-acetylated histone H4 ChIP.

results because of integration of the BCR-ABL construct at DNA regions critical for 14-3-3 promoter epigenetic regulation, PCR was performed only in K562 cell line. 14-3-3 Sigma promoter acetylation was significantly lowered at 4 h of IM exposure and further reduced thereafter (Figure 4B).

To confirm that 14-3-3 sigma promoter hyper-acetylation is an event associated with p210 BCR-ABL TK *in vivo*, we used early CD34+ myeloid progenitors purified from the peripheral blood of two normal controls (apheresis intended for bone marrow transplantation) and two CML patients at diagnosis. In all cases CD34+ cell content measured by means of flow cytometric analysis was >90%. Moreover, FISH analysis allowed the detection of BCR-ABL rearranged gene in >80% of CD34+ cells from CML patients (data not shown). PCR amplification of DNA from ChIP products confirmed 14-3-3 sigma promoter-enhanced acetylation in CD34+ cells from CML patients compared with normal controls (Figure 4B). Moreover, semi-quantitative PCR on CD34+ cells from one CML patient confirmed significant reduction of 14-3-3 sigma transcripts following *in vitro* exposure to IM (1 μM) (Figure 4A).

Informational spectrum method (ISM) and cross-spectrum (CS) analysis pinpoint 14-3-3 sigma and c-ABL mutual interactions

ISM is a virtual spectroscopy method for functional analysis of protein interactions based on their structure (9,10).

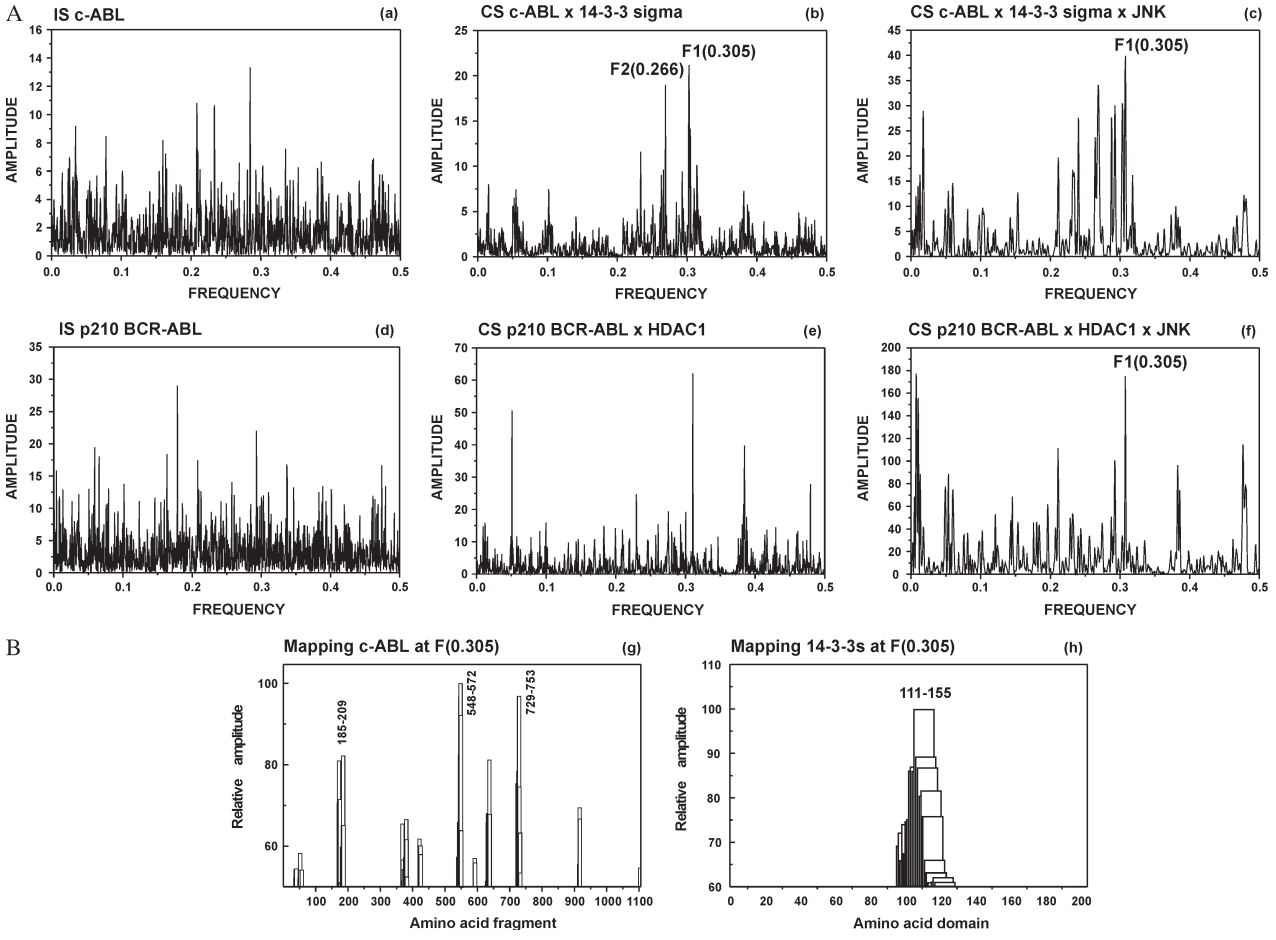

Figure 5: ISM and CS analysis of cABL and 14-3-3 sigma. A) Upper panel: CS between c-ABL and 14-3-3 sigma frequencies from the Fourier transform of the sequence of electron-ion interaction potential corresponding to the amino-acid sequence of the protein are put in abscissa axis. The lowest frequency is 0.0 and the highest is 0.5. The amplitudes, in arbitrary units corresponding to each frequency component in the informational spectrum, are put in ordinate axis. Middle panel: Computation mapping of c-ABL binding site on 14-3-3 sigma based on ISM analyses of 45 amino acids long overlapping fragments with one residue shift. Systematic scanning shows that amino acid domain spanning residues 111–155 in 14-3-3 sigma mostly contributes to the amplitude corresponding to *F*1 (0.3056). Lower panel: Computation scanning shows three domains spanning residues 185–209, 548–572 and 729–753 in c-ABL contributing to the *F*1 frequency. The ordinate axis in middle and lower panels represents amplitudes, in arbitrary units, normalized on the maximal amplitude value. B) CS of JNK with c-ABL/14-3-3 sigma complex (upper panel) and p210 BCR-ABL/HDAC1 complex (lower panel). See legend to section A—upper panel for details.

Briefly, the information encoded by protein primary structures, represented by common frequency component(s) in their IS and mathematical filtering in CS profiles, allowed identification of specific recognition sites relevant for protein binding. Individual 14-3-3 sigma and c-ABL IS and their CS revealed two dominant peaks at Fourier frequencies *F*1 (0.3056) and *F*2 (0.2666) (see Supporting Information, Figure S1). In previous studies we demonstrated that the dominant peak at a given frequency distinguishes the amino-acid domain mostly contributing to protein binding (10,22,23). Accordingly, CS confirmed that 14-3-3 sigma and c-ABL interaction encompasses protein sequences represented by *F*1 frequency (Figure 5A, upper panel). Fragments involved in two-protein interaction were identified by means of peptide scanning of the entire sequence by the ISM algorithm. In 14-3-3 sigma the amplitude of *F*1 frequency is determined by a domain spanning residues 111–155 (Figure 5A, middle panel). Interestingly, this domain encompasses seven out of nine residues (Asp^{126}, Tyr^{127}, Arg^{129}, Tyr^{130}, Leu^{131}, Ala^{132} and Tyr^{151}) previously identified as the 14-3-3 binding site (24). In c-ABL three domains spanning residues 185–209, 548–572 and 729–753 contribute to *F*1 frequency amplitude (Figure 5A, lower panel). Notably, the last domain includes the Thr^{735} residue involved in c-ABL ligand to 14-3-3 sigma (8).

Further ISM analyses showed that c-ABL and p210 BCR-ABL exhibit significant differences in CS profiles (see Supporting Information, Figure S1). Conversely, c-ABL/14-3-3 sigma complex has a spectral profile similar to p210 BCR-ABL/HDAC1 complex described in our previous study (see Supporting Information, Figure S2) (11). CS of c-ABL/14-3-3 sigma and p210 BCR-ABL/HDAC1 complexes with JNK exhibited the same dominant peak at *F*1 frequency (0.3056) (Figure 5B). However, the peak amplitude of p210 BCR-ABL/HDAC1/JNK complex (149.44) was significantly higher compared with that of c-ABL/14-3-3 sigma/JNK complex (39.91) (Figure 5B). The findings suggest that JNK stronger ligand to p210 BCR-ABL/HDAC1 complex may hinder its targeting to c-ABL/14-3-3 complex.

Discussion

P210 BCR-ABL oncogenic potential mostly arises from the constitutive activation of ABL TK by BCR sequences (1). In consequence of its cytoplasmic location, the fusion protein conveys proliferation and survival signals by interacting with multiple transduction pathways and usurps c-ABL TK physiological functions that require protein nuclear relocation (2). Accordingly, p210 BCR-ABL TK drives CML cells towards apoptotic death when allowed to translocate into the nuclear compartment by IM and entrapped there by leptomycin B [which blocks CRM1(exportin 1) nuclear export signal (NES) receptor] (3). However, the cause of disruption of not-rearranged, normal c-ABL function associated with p210 BCR-ABL TK remains elusive.

The activation of p145 c-ABL protein in response to DNA damage is driven by interactions of its SH3 domain with a DPAPNPPHFP motif (residues 1373–1382) of ATM and phosphorylation at Ser^{465} in the TK domain (25,26). C-ABL pro-apoptotic and anti-proliferative effects are promoted by mechanisms partly dependent on p53 and its homologue p73, and conditional upon its nuclear import, following release from the cytoplasmic 14-3-3 scaffolding proteins (zeta and sigma) phosphorylated at $Ser^{184/186}$ by JNK (8). Here we demonstrated that p210 BCR-ABL TK precludes the release of not-rearranged c-ABL from 14-3-3 sigma in response to DNA damage by preventing 14-3-3 sigma and JNK phosphorylation (Figure 1). The inhibition of fusion protein TK by IM is followed by 14-3-3 sigma phosphorylation at Ser^{186} (corresponding to Ser^{184} in 14-3-3 zeta), JNK phosphorylation at Thr^{183} (adjacent to Ser^{184} residue involved in 14-3-3 phosphorylation), c-ABL release and nuclear import (Figure 2A). The last two events may be concurrently promoted by c-ABL dephosphorylation at Ser-containing motifs critical for binding to 14-3-3 (Figure 2A) (17). Experiments with the 14-3-3 antagonist R18, a peptide masking 14-3-3 region required for client protein binding, confirmed the role of 14-3-3 sigma ligand in c-ABL cytoplasmic compartmentalization associated with p210 BCR-ABL TK (18). C-ABL nuclear import was, in fact, promoted by R18 alone and further enhanced by IM-induced 14-3-3 sigma phosphorylation (Figure 2B,C). As expected, apoptotic death, the major consequence of c-ABL nuclear targeting, was significantly increased by exposure to IM and R18 alone and further augmented by their combination (Figure 2D).

A further role of c-ABL in cell response to DNA damage arises from its targeting to mitochondrial membranes and phosphorylation of initiator caspase-9; both events are attenuated by IM-induced inhibition of c-ABL TK (27–30). Notably, c-ABL nuclear translocation in response to DNA is independent from its TK activity and, in addition, higher IM concentrations (10 μM) than those used in this study (1 μM) are required to preclude mitochondrial integrity destruction by c-ABL (27–29).

Over-expression of 14-3-3 associated with p210 BCR-ABL TK likely contributes to retaining p145 c-ABL protein in the cytoplasm (Figure 1). It is driven by epigenetic mechanisms encompassing histone H4 hyper-acetylation at a 14-3-3 promoter conserved region critical for gene transcription (21). Accordingly, p210 BCR-ABL TK inhibition by IM is followed by persistent histone H4 de-acetylation at 14-3-3 sigma promoter and significant reduction of 14-3-3 sigma transcript and protein (Figures 4A,B). Experiments carried on CD34+ haematopoietic progenitors purified from healthy persons and CML patients at clinical diagnosis confirmed that histone H4 hyper-acetylation at 14-3-3 sigma promoter leading to 14-3-3 over-expression is an event associated with BCR-ABL expression in vivo (Figure 4A,B). Further investigation is required to elucidate whether HDAC1, whose cytoplasmic compartmentalization in a complex tethered by p210 BCR-ABL TK has a role in BCR promoter acetylation status and BCR-ABL

transcription, is involved in 14-3-3 sigma promoter hyper-acetylation and transcriptional activation (11).

ISM and CS analyses identified specific recognition sites relevant for c-ABL and 14-3-3 sigma mutual interaction at Fourier frequency F1 (0.3056) (Figure 5A, upper panel; supplementary section, Figure S1). Peptide scanning by the ISM algorithm allowed to distinguish a 14-3-3 sigma domain involved in c-ABL interaction at a region spanning residues 111–155 (Figure 5A, middle panel). Interestingly, this domain encompasses seven out of nine residues (Asp^{126}, Tyr^{127}, Arg^{129}, Tyr^{130}, Leu^{131}, Ala^{132} and Tyr^{151}) previously identified as 14-3-3 binding sites (17). In c-ABL three regions encompassing residues 185–209, 548–572 and 729–753 contribute to protein interaction with 14-3-3 sigma (Figure 5A, lower panel). Notably, the last region includes Thr^{735} whose phosphorylation is mandatory for 14-3-3 ligand (8).

Our results ascribe to JNK a major role in 14-3-3 sigma phosphorylation allowing c-ABL release and nuclear import after p210 BCR-ABL TK inhibition (Figures 2A). In fact, in BCR-ABL-expressing cells JNK inhibitor attenuates 14-3-3 sigma phosphorylation at Ser^{186} and c-ABL nuclear import in response to IM (Figure 3A). CS profiles suggest that a greater affinity of JNK for a HDAC1-containing complex tethered by p210 BCR-ABL TK may interfere with JNK targeting to c-ABL/14-3-3 complex (Figure 5B) (11). Accordingly, HDAC inhibitors enhance IM pro-apoptotic effects in BCR-ABL-expressing cells through mechanisms involving JNK activation (31–33). Furthermore, we found that p38 MAPK, a critical effector of IM anti-leukemic effects in CML, contributes to 14-3-3 sigma phosphorylation (34). In fact, p38 MAPK inhibition in BCR-ABL-expressing cells significantly reduced 14-3-3 sigma phosphorylation at Ser^{186} in response to IM (Figure 3A). A previous study showed that p38 MAPK activation inhibits the dimerization of a 14-3-3 isoform (zeta) leading to client protein ligand de-stabilization through mitogen-activated protein kinase-activated protein kinase 2 (MAPKAPK2)-induced phosphorylation at Ser^{58}, a not conserved residue in 14-3-3 sigma (20). Further investigation is required to define the interactions of p38 MAPK and downstream effectors with Ser^{186} residue in 14-3-3 sigma.

14-3-3 Phosphorylation is not the only cause of c-ABL relocation following p210 BCR-ABL TK inhibition. In fact, c-ABL nuclear import in response to IM is decreased, but not completely abolished by JNK and p38 MAPK inhibitor-induced reduction of 14-3-3 sigma phosphorylation (Figure 3A). The findings that JNK and p38 MAPK inhibitors preclude complete c-ABL de-phosphorylation and 14-3-3 sigma reduction in response to IM support that c-ABL phosphorylation status and 14-3-3 sigma expression levels may play a role in the two-protein ligand (Figure 3A). Furthermore, c-ABL release from 14-3-3 and nuclear import are not the only events involved in apoptotic death of BCR-ABL-expressing cells. In fact, in clone 3B at 33°C JNK and p38 MAPK inhibitors respectively enhanced and left steady the apoptotic cell fraction in spite of c-ABL persistent retention in the cytoplasm and reduced nuclear translocation (Figure 3B).

Finally, we confirmed p210 BCR-ABL TK exclusive location in the cytoplasm (Figure 2A). The fusion protein nuclear translocation, resulting in the disruption of ATR signalling and radio-resistant DNA synthesis (RDS), was only reported in response to etoposide (35). P210 BCR-ABL cytoplasmic compartimentalization has been ascribed to a more rapid nuclear export rather than precluded nuclear import (3). The absence of p210 BCR-ABL/14-3-3 sigma co-immunoprecipitation signals seems to exclude that the fusion protein is retained in the cytoplasm by 14-3-3 binding to BCR through 14-3-3-related protein BAP-1 (data not shown) (36). A recent study proved that MUC1 (a trans-membrane glycoprotein that stabilizes p210 BCR-ABL by directly binding the BCR N-terminal region) blocks ABL phosphorylation at a conserved residue (Thr^{735}) required for 14-3-3 ligand, further supporting that p210 BCR-ABL can not bind 14-3-3 (37,38).

In conclusion, here we demonstrate that p210 BCR-ABL TK precludes c-ABL physiological functions by preventing the chain of events that let its release from 14-3-3 scaffolding proteins (Figure 6). Our study supports the advantage of 14-3-3 ligand targeting in CML therapy proceeding from restored functions of not-rearranged c-ABL and other 14-3-3 client proteins, such as FOXO3a, BAD and BIM, involved in disease pathogenesis and progression (39).

Materials and Methods

Cells and treatments

A ts BCR-ABL mutant subcloned into a pDG retroviral vector under the control of myeloproliferative sarcoma virus LTR promoter along with the neomycin resistance gene has been expressed in murine myeloid progenitor cell line 32D through electroporation. A ts BCR-ABL-transduced clone 3B generated from a single colony grown in methylcellulose and selected in medium in addition to the neomycin analogue G418 (500 μg/mL from Sigma) was preliminarily assayed for the temperature dependence of its p210 protein TK activity (39). It was maintained in RPMI 1640 (Roswell Park Memorial Institute) medium supplemented with 10% fetal calf serum (FCS, from Gibco), 1% l-Glutamine, antibiotics and 10% WEHI-3 conditioned medium (CM) as source of IL-3 when required in 5% CO_2 and fully humidified atmosphere at either permissive (33°C) or non-permissive (39°C) temperature for p210 BCR-ABL TK activity. Parental 32D cell line was maintained at 37°C in RPMI medium in addition to FCS, 10% WEHI-3 CM and antibiotics. Human CML cell line K562 was maintained at 37°C in RPMI in addition to FCS, l-Glutamine and antibiotics. C-ABL sub-cellular relocation in response to IR was evaluated at 3rd h from exposure to low dose (4 Gy), low dose rate (0.05 Gy/min) gamma irradiation under a ^{60}CO source. Clone 3B and K562 cell sensitivity to IM (provided by Novartis Institutes for Biomedical Research, Oncology, Basel, SW) was preliminarily measured in clonogenic assays (0.9% methylcellulose in addition to 30% FCS). One micromolar IM was used to investigate the time-course induction of signals involved in sub-cellular relocation of c-ABL protein. A 24 h *in vitro* exposure of clone 3B at 33°C and K562 cells to 25 μM R18 peptide (BIOMOL International, Plymouth Meeting, PA, USA) alone or in combination with 1 μM IM was used to investigate the role of 14-3-3 binding site in c-ABL ligand (18). JNK

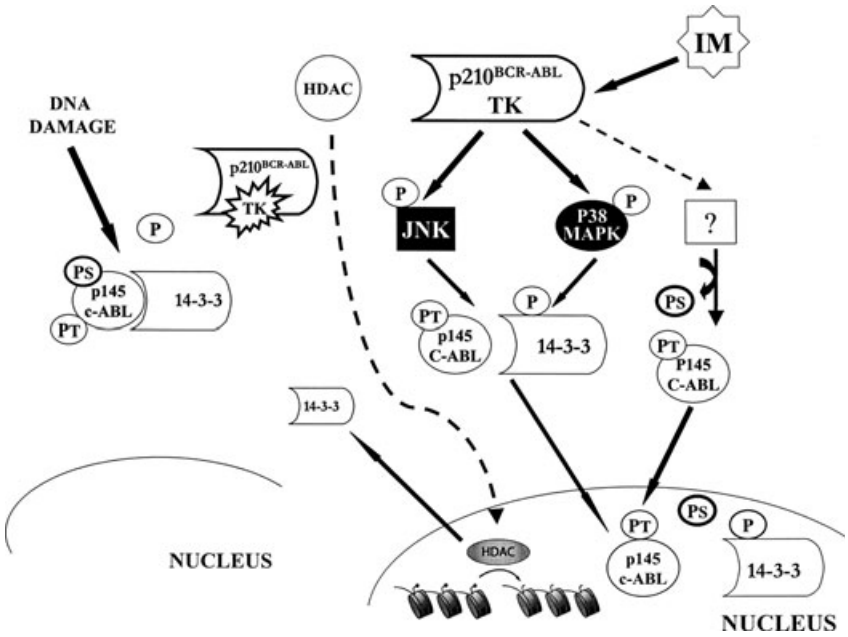

Figure 6: Cytoplasmic location of p210 BCR-ABL precludes c-ABL physiological functions, as mediator of apoptotic cell death after DNA damage, by preventing the chain of events that let its release from 14-3-3 scaffolding proteins.

and p38 MAPK inhibitors (JNK inhibitor IX and SB202190) were used at 20 μM concentration either alone or in combination with 1 μM IM.

Protein analysis

Western blot and immunoprecipitation (IP)/immunoblotting analyses were performed on whole cell and nuclear lysates according to published methods (40). Anti-ABL SH2, anti 14-3-3 sigma antibodies were purchased from Upstate Biotechnology; antibodies anti-phosphorylated ABL (Tyr^{245}), anti-phopshorylated 14-3 3 sigma (Ser^{186}), anti-p38 MAPK, anti-phosphorylated p38 MAPK (Thr^{180}) and anti-JNK and anti-phosphorylated JNK (Thr^{183}) were purchased from Cell Signalling and anti-actin and anti-histone H1 antibodies were purchased from Santa Cruz Biotechnology. Contamination of nuclear lysates by cytoplasmic proteins and of whole cell lysates by nuclear proteins was excluded by histone H1 and beta actin labelling (data not shown). Signal intensities in single blots from three repeated experiments were measured by a GS-700 imaging densitometer (Bio-Rad) equipped with a dedicated software (Molecular Analyst, Bio-Rad). Statistical significance of differences among signal intensities was calculated by means of *t* student.

Chromatin was obtained from 1×10^7 cells of clone 3B and K562 cell line following 10 minutes exposure to 1% formaldehyde (to crosslink histones and DNA) using a commercial kit (from Quiagen). It was immunoprecipitated with an anti-acetylated histone H4-ChIP grade antibody (Upstate Biotechnology). Histone H4 acetylation status of a 14-3-3 promoter region critical for gene transcription relative to histone H4 acetylation as internal control was investigated by means of PCR on DNA purified from 20 μL of anti-Ac H4 chromatin immunoprecipitation products (ChIP) which had the histone-DNA crosslink reversed by heating at 65°C for 4 h. Specific primer pairs were designed to amplify a 263 bp sequence within the 14-3-3 promoter region (5′ TGGAAGGGCACTGTGAAAGT 3′ and 5′ GAGAAGGGTGGGGAGGAGCA 3′) and a 325 bp sequence within the histone H4 promoter (5′ CTATTCTCTCACTTGCTCTTG 3′ and 5′ GTCCCTGGCGCTTAAGCGCG 3′). PCR conditions (40 cycles of 0′′ at 95°C, 0′′ at 59°C and 25′′ at 72°C) were set to enable the evaluation of 14-3-3 sigma promoter acetylation status in capillaries using an Idaho instrument. Signal intensities were quantified by a GS-700 imaging densitometer and a dedicated software (Bio-Rad). *T* student test served to evaluate statistical significance of differences among PCR signal intensities in three repeated experiments.

RNA analysis

Total RNA extraction was performed using a commercial kit (RNeasy from Qiagen) according to manufacturer instructions. Semi-quantitative PCR used to quantify 14-3-3 sigma expression exploited the ratio between 14-3-3 sigma and housekeeping G3PDH amplification signals resolved in 2% agar and quantified by a GS-700 imaging densitometer (Bio-Rad). Statistical significance of differences among signal intensities was calculated by means of *t* student test. Thirty-five cycles (denaturation at 98°C for 30′′, annealing for 1′ at 58°C, elongation at 72°C for 1′) were carried using the following primers: 5′ GTGTGTCCCCAGAGCCATGG (upper) and 3′ GCACTCATGGCCCTCTTCCA (lower) for 14-3-3 sigma amplification and 5′ TCATCATCTCTGCCCCCTCTG (upper) and 3′ TTCTTCCACCACTTCGTCCGC (lower) for G3PDH amplification.

Cytofluorimetric analysis of apoptosis induction

Cytofluorimetric analysis of apoptotic cell fraction was performed by measuring the uptake of Annexin V (Hoffmann-La Roche, Basel, SW) and propidium iodide (PI) (Sigma) according to published methods (41). Cell fluorescence and PI uptake were measured by means of a FACScan flow cytometer (set at 488 nm excitation and 530 nm bandpass filter wavelength for fluorescein detection or 580 nm for PI detection) and a dedicated software (both from Beckton Dickinson).

Confocal microscopic analysis

C-ABL sub-cellular location was assayed on cells set on poly-L-lysine-coated glass slides, fixed and permeabilized according to published methods (42). Following overnight incubation with primary antibody (from Upstate Biotechnology, 1:500 in PBS and 1% BSA) at 4°C, 1 h incubation at room temperature with secondary antibody [anti-rabbit conjugated with fluorescein isothiocyanate (FITC) from Sigma, 1:2000] and 15′ incubation with 4′,6-diamidino-2-phenylindole (DAPI 1:100 in PBS), slides were analysed under a laser scanning confocal microscopy (MRC 1024 from Bio-Rad) equipped with NIKON Eclipse TE300 with 60x objective lens using LaserSharp2000 and LaserPix softwares (Bio-Rad). Multiple images were acquired using sequential laser excitations at 488 and 568 nm to reduce spectral bleed-through artefacts.

Immuno-magnetic purification of CD34+ cells

$CD34^+$ haematopoietic progenitors were isolated from peripheral blood samples of CML patients at diagnosis and healthy donor apheresis

(intended for bone marrow transplantation) after informed consent. They were obtained by indirect immuno-magnetic labelling (mini-MACS from Milteny Biotech) of mononuclear cell fractions. Their content was measured by means of cytometric analysis with a FacScan (Becton Dickinson).

Fluorescence in situ hybridization (FISH) analysis

FISH was performed using the LSI BCR-ABL ES dual Colour Translocation probe (Vysis) according to previously published procedures (11). As many as 20–30 CD34+ cells were scored for the presence of BCR-ABL rearrangement under a fluorescence microscope (Nikon).

The informational spectrum method (ISM)

The ISM encompasses two stages. The first involves the transformation of the amino-acid sequence into a numerical sequence. Each amino acid is represented by the value of the electron-ion interaction potential (EIIP) corresponding to the average energy states of all valence electrons in a particular amino acid. The EIIP values for each amino acid were calculated using the general model pseudopotential: $\langle k+q|w|k\rangle = 0.25Z\sin(\pi 1.04Z)/(2\pi)$, where q is a change of momentum of the delocalized electron in the interaction with potential w, Z_i [$Z = (\Sigma Z_i)/N$], κ the number of valence electrons of the i-th atom of each amino acid and N the total number of atoms in the amino acid. By using discrete Fourier transform (DFT), the numerical sequence was transformed into the frequency domain to create an informational spectrum. DFT is defined as: $X(n) = \Sigma x(m)e^{-j(2/N)nm}$, $n = 1, 2, \ldots, N/2$, where $x(m)$ is the m-th member of a given numerical series, N the total number of points in this series, and $X(n)$ the DFT coefficients. DFT coefficients describe amplitude, phase and frequency of sinusoids of the original signals. The absolute value of complex Fourier transform defines the amplitude spectrum and the phase spectrum. The complete information about the original sequence is contained in both spectral functions. However, the relevant information in the case of protein analysis is provided by the energy density spectrum, defined as: $S(n) = X(n)X^*(n) = |X(n)|^2$, $n = 1, 2, \ldots, N/2$. In this way, individual sequences are considered as discrete signals. As the average distance between amino-acid residues in a polypeptide chain is 3.8 Å, it is assumed that the points into each derived series are equidistant and the distance is arbitrarily set as 1. Then, the maximum frequency in the spectrum is $F = 1/2d = 0.5$.

In order to distinguish common spectral characteristic(s) of two sequences, mathematical filtering was done by multiplying the conjugate complex Fourier transform by the Fourier transform of the target signal: $C(n) = S_1(n)S^*{}_2(n)$ $n = 1, 2, \ldots, N/2$. The result of multiplication is a CS function. The prominent peak in this function denotes common frequency component(s) of explored proteins. The numerical series derived from analysed sequences are normalized to zero mean and zero padded to produce a vector equal in length to the smallest power of 2 greater than (or equal to) the largest domain in the data set. Padding with zeros is itself a standard practice in Fourier analysis when using a discrete fast Fourier transform-based algorithm, as the length of the input patterns are required to be a power of two. The zero padding induces an increase of the spectrum resolution without consequence on the characteristic frequency.

Computational mapping of ligand-binding site

ISM was used to map applied c-ABL binding site to 14-3-3 sigma. Peptide scanning was used to define linear protein fragments which mostly contribute to the amplitude at the characteristic frequency and therefore are responsible for interaction(s) described by the particular spectral characteristic. The entire sequences of 14-3-3 sigma were scanned by the ISM algorithm as 25 and 45 amino acids long, overlapping polypeptides with one residue shift, which led to the identification of the region with the highest amplitudes at predefined Fourier frequency $F1$ (0.3056).

Acknowledgments

This study was supported by grants from the University of Bologna (ex60% funds), BolognaAIL and Carisbo Foundation. M.M. is a Postdoctoral fellow of Dipartimento di Scienze Radiologiche e Istocitopatologiche (University of Bologna–Medical School). P.C. is the recipient of a grant from Centro Interdipartimentale di Ricerca sul Cancro 'Giorgio Prodi'. The Authors declare no competing financial interest.

Supporting Information

Additional Supporting Information may be found in the online version of this article:

Figure S1: ISM of 14-3-3 sigma, c-ABL and p210 BCR-ABL. The frequencies from Fourier transform of the sequence of electron-ion interaction potential corresponding to the amino-acid sequence of the proteins are represented in abscissa axis. The amplitudes, in arbitrary units, corresponding to each frequency component of the IS are represented in the ordinate axis.

Figure S2: CS profiles of p210 BCR-ABL/HDAC1 and c-ABL/14-3-sigma profiles. Please note: Wiley-Blackwell are not responsible for the content or functionality of any supporting materials supplied by the authors. Any queries (other than missing material) should be directed to the corresponding author for the article.

References

1. McWhirter JR, Galasso DL, Wang JY. A coiled-coil oligomerization domain of Bcr is essential for the transforming function of Bcr-Abl oncoproteins. Mol Cell Biol 1993;13:7587–7595.
2. Shaul Y. c-Abl: activation and nuclear targets. Cell Death Differ 2000;7:10–16.
3. Vigneri P, Wang JY. Induction of apoptosis in chronic myelogenous leukemia cells through nuclear entrapment of BCR-ABL tyrosine kinase. Nat Med 2001;7:228–234.
4. Dai Z, Quackerbush RC, Courtney KD, Grove M, Cortez D, Reuther GW, Pendergast AM. Oncogenic Abl and Src tyrosine kinases elicit the ubiquitin-dependent degradation of target proteins through a Ras-independent pathway. Genes Dev 1998;12:1415–1424.
5. Asimakopoulos FA, Shteper PJ, Krichvsky S, Fibach E, Pollack A, Rachmilewitz E, Ben-Neriah Y, Ben-Yehuda D. ABL1 methylation is a distinct molecular event associated with clonal evolution of chronic myeloid leukaemia. Blood 1999;94:2452–2460.
6. Kharbanda S, Yuan ZM, Weichselbaum R, Kufe D. Determination of cell fate by c-Abl activation in the response to DNA damage. Oncogene 1998;17:3309–3318.
7. Wang JY. Controlling Abl: auto-inhibition and co-inhibition?. Nat Cell Biol 2004;6:3–7.
8. Yoshida K, Yamaguchi T, Natsume T, Kufe D, Miki Y. JNK phosphorylation of 14-3-3 proteins regulates nuclear targeting of c-Abl in the apoptotic response to DNA damage. Nat Cell Biol 2005;7:278–285.
9. Veljkovic V, Cosic I, Dimitrijevic B, Lalovic D. Is it possible to analyze DNA and protein sequences by the methods of digital signal processing?. IEEE Trans Biomedical Eng 1985;32:337–341.
10. Doliana R, Veljkovic V, Prljic J, Veljkovic N, De Lorenzo E, Mongiat M, Ligresti G, Marastoni S, Colombatti A. EMILINs interact with anthrax protective antigen and inhibit toxin action in vitro. Matrix Biol 2007;27:96–106.
11. Brusa G, Zuffa E, Mancini M, Benevenuti M, Calonghi N, Barbieri E, Santucci MA. P210 Bcr-abl tyrosine kinase interaction with histone

deacetylase 1 modifies histone H4 acetylation and chromatin structure of chronic myeloid leukaemia haematopoietic progenitors. Br J Haematol 2006;132:359–369.
12. Kharbanda S, Ren R, Pandey P, Shafman TD, Feller SM, Weichselbaum RR, Kufe DW. Activation of the c-Abl tyrosine kinase in the stress response to DNA-damaging agents. Nature 1995;376:785–788.
13. Smith KM, Yacobi R, van Etten RA. Autoinhibition of Bcr-Abl through its SH3 domain. Mol Cell 2003;12:27–37.
14. Muslin AJ, Xing H. 14-3-3 proteins: regulation of subcellular localization by molecular interference. Cell Signal 2000;12:703–709.
15. Fleming Y, Armstrong CG, Morrice N, Paterson A, Goedert M, Cohen P. Synergistic activation of stress-activated protein kinase1/c-Jun-terminal kinase (SAPK1/JNK) isoforms by mitogen-activated protein kinase 4 (MKK4) and MKK7. Biochem J 2000;352:145–154.
16. Tzivion G, Avruch J. 14-3-3 proteins: active cofactors in cellular regulation by serine/threonine phosphorylation. J Biol Chem 2002;277:3061–3064.
17. Muslin AJ, Tanner JW, Allen PM, Shaw AS. Interaction of 14-3-3 with signalling proteins is mediated by the recognition of phosphoserine. Cell 1996;84:889–897.
18. Masters SC, Fu H. 14-3-3 proteins mediate an essential anti-apoptotic signal. J Biol Chem 2001;276:45193–45200.
19. Yoshida K, Miki Y. Enabling death by the Abl tyrosine kinase: mechanisms for nuclear shuttling of c-Abl in response to DNA damage. Cell Cycle 2005;4:777–779.
20. Powell DW, Rane MJ, Joughin BA, Kalmukova R, Hong JH, Tidor B, Dean WL, Pierce WM, Klein JB, Yaffe MB, McLeish KR. Proteomic identification of 14-3-3zeta as a mitogen-activated protein kinase-activated protein kinase 2 substrate: role in dimmer formation and ligand binding. Mol Cell Biol 2003;23:5376–5387.
21. Lodygin D, Hermeking H. The role of epigenetic inactivation of 14-3-3 sigma in human cancer. Cell Res 2005;15:237–246.
22. Veljkovic V, Metlas R. Identification of nanopeptide from HTLV-III, ARV-2 and LAVBRU envelope gp120 determining binding to T4 cell surface protein. Cancer Biochem Biophys 1988;10:91–106.
23. Pham TD. LPC cepstral distortion measure for protein sequence comparison. IEEE Trans Nanobioscience 2006;5:83–88.
24. Wilker EW, Grant RA, Artim SC, Yaffe MB. A structural basis for 14-3-3 sigma functional specificity. J Biol Chem 2005;280:18891–18898.
25. Shafman T, Khanna KK, Kedar P, Spring K, Kozlov S, Yen T, Hobson K, Gatei M, Zhang N, Watters D, Egerton M, Shiloh Y, Kharbanda S, Kufe D, Lavin MF. Interaction between ATM protein and c-Abl in response to DNA damage. Nature 1997;387:520–523.
26. Baskaran R, Wood LD, Whitaker LL, Canman CE, Morgan SE, Xu Y, Barlow C, Baltimore D, Wynshaw-Boris A, Kastan MB, Wang JY. Ataxia telangiectasia mutant protein activates c-Abl tyrosine kinase in response to ionizing radiation. Nature 1997;387:516–519.
27. Kumar S, Bharti A, Mishra NC, Raina D, Kharbanda S, Saxena S, Kufe D. Targeting of the c-Abl tyrosine kinase to mitochondria in the necrotic cell death response to oxidative stress. J Biol Chem 2001;276:17281–17285.
28. Ito Y, Pandey P, Mishra N, Kumar S, Narula N, Kharbanda S, Saxena S, Kufe D. Targeting the c-Abl tyrosine kinase to mitochondria in endoplasmic reticulum stress-induced apoptosis. Mol Cell Biol 2001;21:6233–6242.
29. Kumar S, Mishra N, Raina D, Saxena S, Kufe D. Abrogation of the cell death response to oxidative stress by the c-Abl tyrosine kinase inhibitor STI571. Mol Pharmacol 2003;63:276–282.
30. Raina D, Pandey P, Ahmad R, Bharti A, Ren J, Kharbanda S, Weichselbaum R, Kufe D. c-Abl tyrosine kinase regulated caspase-9 autocleavage in the apoptotic response to DNA damage. J Biol Chem 2005;280:11147–11151.
31. Yu C, Subler M, Rahmani M, Reese E, Krystal G, Conrad D, Dent P, Grant S. Induction of apoptosis in BCR/ABL+ cells by histone deacetylase inhibitors involves reciprocal effects on the RAF/MEK/ERK and JNK pathways. Cancer Biol Ther 2003;2:544–551.
32. Nimmanapalli R, Fuino L, Stobaugh C, Richon V, Bhalla K. Cotreatment with the histone deacetylase inhibitor suberoylanilide hydroxamc acid (SAHA) enhances Imatinib-induced apoptosis of Bcr-Abl-positive human acute leukaemia cells. Blood 2003;101:32136–32139.
33. Yu C, Rahmani M, Almenara J, Subler M, Krystal G, Conrad D, Varticovski L, Dent P, Grant S. Histone deacetylase inhibitors promote STI571-mediated apoptosis in STI571-sensitive and—resistant Bcr/Abl + human myeloid leukaemia cells. Cancer Res 2003;63:2118–2126.
34. Parmar S, Katsoulidis E, Verma, Sassano A, Lal L, Majchrzak B, Ravandi F, Tallman MS, Fish EN. Role of the p38 mitogen-activated protein kinase pathway in the generation of the effects of imatinib mesylate (STI571) in BCR-ABL-expressing cells. J Biol Chem 2004;279:25345–25352.
35. Dierov J, Dierova R, Carroll M. BCR/ABL translocates to the nucleus and disrupts an ATR-dependent intra-S phase checkpoint. Cancer Cell 2004;5:275–285.
36. Reuther GW, Fu H, Cripe LD, Collier RJ, Pendergast AM. Association of the protein kinases c-Bcr and Bcr-Abl with proteins of the 14-3-3 family. Science 1994;266:129–133.
37. Kawani T, Ito M, Raina D, Wu Z, Rosenblatt J, Avigan D, Stone R, Kufe D. MUC1 oncoprotein regulates Bcr-Abl stability and pathogenesis in Chronic Myelogenous Leukemia. Cancer Res 2007;67:11576–11584.
38. Raina D, Ahmad R, Kumar S, Ren J, Yoshoda K, Kharbanda S, Kufe D. MUC1 oncoprotein blocks nuclear targeting of c-Abl in the apoptotic response to DNA damage. EMBO J 2006;25:3774–3783.
39. Dong S, Kang S, Lonial S, Khoury H J, Viallet J, Chen J. Targeting 14-3-3 sensitizes native and mutant BCR-ABL to inhibition with U0126, rapamycin and Bcl-2 inhibitor GX15-070. Leukemia 2008;22(3):572–7 Epub ahead of print.
40. Mazzacurati L, Pattacini L, Brusa G, Mancini M, Benvenuti M, Barbieri E, Martinelli G, Baccarani M, Greenberger JS, Santucci MA. Chk2 drives late G1/early S phase arrest of clonal myeloid progenitors expressing the p210 BCR-ABL tyrosine kinase in response to STI571. Hematol J 2004;5:168–177.
41. Mancini M, Brusa G, Zuffa E, Corrado P, Martinelli G, Grafone T, Barbieri E, Santucci MA. Persistent Cdk2 inactivation drives growth arrest of BCR-ABL-expressing cells in response to dual inhibitor of SRC and ABL kinases SKI606. Leuk Res 2007;31:979–987.
42. Mancini M, Calonghi N, Pagnotta E, Masotti L, Brusa G, Zuffa E, Calabrò A, Barbieri E, Santucci MA. P210 BCR-ABL tyrosine kinase prevents apoptotic cell death through multiple pathways converging at mitichondrial membranes. Gene Ther Mol Biol 2005;9:359–370.